

1 **Electrical conductivity of anhydrous and hydrous gabbroic melt**
2 **under high temperature and high pressure: Implications for the**
3 **high conductivity anomalies in the region of mid-ocean ridge**

4 Mengqi Wang^{1,2}, Lidong Dai^{1*}, Haiying Hu^{1*}, Ziming Hu^{1,2}, Chenxin Jing^{1,2}, Chuanyu
5 Yin^{1,2}, Song Luo^{1,2} and Jinhua Lai^{1,2}

6 ¹*Key Laboratory of High-temperature and High-pressure Study of the Earth's*
7 *Interior, Institute of Geochemistry, Chinese Academy of Sciences, Guiyang, China*

8 ²*University of Chinese Academy of Sciences, Beijing, China*

9 To be submitted to *Solid Earth*

10 February 26th, 2023

*Authors to whom correspondence should be addressed: dailidong@vip.gyig.ac.cn and huhaiying@vip.gyig.ac.cn

Abstract

11
12 The electrical conductivity of gabbroic melt with four different water contents (i.e.
13 0, 2.59 wt%, 5.92 wt% and 8.32 wt%) was measured at temperatures of 873–1373 K
14 and pressures of 1.0–3.0 GPa using YJ–3000t multi–anvil high–pressure apparatus and
15 Solartron–1260 impedance spectroscopy analyzer. At a fixed water content of 2.59 wt%,
16 the electrical conductivity of the sample slightly decreased with increasing pressure at
17 the temperature range of 873–1373 K, and its corresponding activation energy and
18 activation volume were determined as 0.87 ± 0.04 eV and -1.98 ± 0.02 cm³ mole⁻¹,
19 respectively. Under the certain conditions of 873–1373 K and 1.0 GPa, the electrical
20 conductivity of the gabbroic melts tends to gradually increase as the rise of water
21 content from 0 to 8.32 wt%, and the activation enthalpy decreases from 0.93 eV to 0.63
22 eV, accordingly. Furthermore, the functional relation models for the electrical
23 conductivity of gabbroic melts with the variations of temperature, pressure and water
24 content were constructed at high–temperature and high–pressure conditions,
25 respectively. In addition, the dependence relation of the electrical conductivity of melts
26 with the degree of depolymerization was explored under conditions of four different
27 water contents, 1373 K and 1.0 GPa, and three previously available reported results on
28 those of representative calc–alkaline igneous rock melts (i.e. dacitic melt, basaltic melt
29 and andesitic melt) were detailedly compared. In comprehensive combination with our
30 presently acquired electrical conductivity data of gabbroic melt with four different
31 water contents and the available data of polycrystalline olivine, the electrical
32 conductivity of gabbroic melt–olivine system on the variation of volume percentage of

33 anhydrous and hydrous melts was successfully constructed by virtue of the typical
34 Hashin–Shtrikman upper bound model. In light of the electrical conductivity of
35 gabbroic melt–olivine system with the previous MT results, we find that the anhydrous
36 and hydrous gabbroic melts can be employed to reasonably interpret the high
37 conductivity anomalies in the Mohns ridge of the Arctic Ocean.

38 **Keywords: electrical conductivity, gabbroic melt, degree of depolymerization,**
39 **high conductivity anomalies, Mohns ridge**

40 1 Introduction

41 The hydrous melt for various rocks and minerals widely exists at active plate
42 tectonic boundaries such as mid-ocean ridge, subduction zone, orogenic belt, etc. (Shen
43 and Forsyth, 1995; White et al., 2001; Wallace, 2005; Wu et al., 2018; Sim et al., 2020;
44 Förster and Selway, 2021; Li et al., 2022; Turner and Langmuir, 2022). For the typical
45 Mohns ridge in the Arctic Ocean, there existed a large amount of high conductivity
46 anomaly phenomena with its correspondent magnitude of $0.08\text{--}0.32\text{ S m}^{-1}$ for the
47 gabbro-rich regions have been revealed on the basis of previous magnetotelluric (MT)
48 controlled source electromagnetic (CSEM) results (Johansen et al., 2019).

49 Previously available researches have indicated that gabbroic and basaltic melts
50 contain a large amount of water, and the water content for the certain type of melt may
51 be discrepant within the different depth ranges of the oceanic crust (Dixon et al., 1995;
52 Almeev et al., 2008; Shaw et al., 2010; Leuthold et al., 2018). Meanwhile, water content
53 is also considered as a crucial ingredient to possibly affect the electrical conductivity
54 of melt, and there are a large number of previously available reported results for the
55 variation of water content on the electrical conductivity of some representative calc-
56 alkaline igneous rock melts at high temperature and high pressure in the recently several
57 years (Ni et al., 2011; Laumonier et al., 2015; Guo et al., 2017; Chen et al., 2018). For
58 example, Ni et al. (2011) measured the electrical conductivity of hydrous basaltic melt
59 within water content range of 0–6.3 wt% at conditions of 1473–1923 K and 2.0 GPa,
60 and they found that the electrical conductivity of basaltic melt with a fixed water content
61 of 6.3 wt% was of the rough 1.0 order of magnitude higher than that of the anhydrous

62 sample. The electrical conductivity of dacitic melt within the water content range of 0–
63 12 wt% was systematically investigated by Laumonier et al. (2015) within temperature
64 range of 673–1623 K and pressures of 0.3–3.0 GPa. As pointed out by Laumonier et al.
65 (2015), the high conductivity anomalies in the Uturuncu Volcano could be explained
66 by the presence of hydrous dacitic melt. By virtue of a piston cylinder high–pressure
67 apparatus and sweeping–frequency impedance spectroscopy, Guo et al. (2017) obtained
68 the electrical conductivity data of andesitic melt within the water content range of 0.01–
69 5.90 wt% at conditions of 1164–1573 K and 0.5–1.0 GPa. Their experimental results
70 indicated that the presence of less than 20 vol% of hydrous andesitic melt within the
71 water content range of 6–9 wt% can be used to interpret the high conductivity anomalies
72 beneath the surface of the Uturuncu Volcano. Electrical conductivity measurements of
73 the hydrous leucogranitic melt by Chen et al. (2018) at conditions of 739–1680 K and
74 0.36–2.52 GPa were systematically carried out within the water content range of 2.73–
75 11.97 wt%. In comprehensive combination with previous magnetotelluric data in the
76 northwest Himalaya, they considered that water–rich leucogranitic melts with a volume
77 percentage range of 4–16 vol% can be applied to reasonably explain the high
78 conductivity anomalies in these regions.

79 For the natural gabbroic rock, some previously available electrical conductivity
80 results were obtained using the piston–cylinder and multi–anvil high–pressure
81 apparatus at high temperature and high pressure. Sato and Ida (1984) measured the
82 electrical conductivity of the olivine–gabbro containing gabbroic melt at the
83 temperature range from 1123 K to 1473 K and atmospheric pressure, and the effects of

84 ionic diffusion of charge carriers (i.e. sodium, iron, magnesium and/or calcium ions)
85 and geometric structure of melt on the electrical conductivity of olivine–gabbro samples
86 were detailedly explored. The measurements of electrical conductivity for natural
87 gabbro were carried out at conditions of 1023–1423 K and room pressure by Schilling
88 et al. (1997), and they proposed that the electrical conductivity of samples can be
89 enhanced by the increasing volume percentage of gabbroic melt. As for the natural
90 Oman gabbro, the electrical conductivity of gabbroic melt with the volume percentage
91 proportion of 34 % was ~1.0–2.0 orders of magnitude higher than that of melt–free
92 sample within the temperature range from 1073 K to 1523 K and pressures of 0.3–1.0
93 GPa (Maumus et al., 2005). However, the influence of water content on the electrical
94 conductivity of gabbroic melt at high temperature and high pressure was not
95 investigated in detail. Consequently, it is crucial to make a systematic investigation on
96 the electrical conductivity of gabbroic melt with different water contents at high–
97 temperature and high–pressure conditions.

98 In the present studies, a series of electrical conductivity on the gabbroic melts were
99 systematically performed under conditions of 873–1373 K, 1.0–3.0 GPa and the
100 variation of water content range from 0 to 8.32 wt%. The effects of temperature,
101 pressure and water content on the electrical conductivity of gabbroic melt are deeply
102 explored, and the functional relation models have been successfully established at high–
103 temperature and high–pressure conditions. In conjunction with the degree of
104 depolymerization, the electrical conductivity of gabbroic melt with different water
105 contents is compared with that of three representative calc–alkaline igneous rock melts

106 (i.e. dacitic melt, andesitic melt and basaltic melt). Based on the calculated electrical
107 conductivity of gabbroic melt–olivine system, its potential geophysical implication was
108 detailedly discussed in the Mohns ridge of the Arctic Ocean.

109 **2 Experimental procedures**

110 **2.1 Sample Preparation**

111 The natural gabbroic rock used in this study was collected from the ophiolite suite
112 in the region of Ganzi Tibetan autonomous prefecture, Sichuan province, China. By
113 virtue of the high–temperature quenched melt for the natural rock powder, the
114 anhydrous and hydrous gabbroic melts are successfully obtained. Firstly, the fresh
115 natural gabbro was finely crushed and ground into the sample powder with the grain
116 size of less than 50 μm in an agate mortar. Then, the sample powder was kept in the
117 furnace at 473 K to remove the absorbed water. To obtain the homogeneously initial
118 materials for the subsequent electrical conductivity measurement, the powder of
119 gabbroic rock was melted at the temperature of 1473 K for 1.5 hours and rapidly
120 quenched in a high–temperature muffle furnace. Further, gabbroic melt was crushed
121 and ground again into powder with a grain size less than 50 μm and stored in a vacuum
122 dry furnace at 373 K. To synthesize the hydrous gabbroic melt, the desired amount of
123 deionized water was added to the powder, and subsequently, the sample encapsulated
124 in a gold tube using the Lampert–Puk precise welding device. After that, the starting
125 hydrous gabbroic melts with different water contents were synthesized at conditions of
126 1373 K and 1.0–3.0 GPa for 12 hours in the YJ–3000t multi–anvil high–pressure
127 apparatus, and all of these obtained samples are homogeneous without any available

128 crystals or bubbles. Detailed hot-pressed sintering assemblage was similar to that
129 previously described by Hu et al. (2022a). Lastly, all of the gabbroic melts were
130 polished into cylinders with diameters of ~4.0–5.0 mm and heights of ~4.0–6.0 mm,
131 and kept in muffle furnace at 423 K for 10 hours to eliminate the absorbed water for
132 subsequent electrical conductivity measurements. The chemical compositions of
133 anhydrous and hydrous gabbroic melts were analyzed by virtue of the electronic probe
134 microscopy analysis (EPMA) at the State Key Laboratory of Ore Deposit Geochemistry,
135 Institute of Geochemistry, Chinese Academy of Sciences, Guiyang, China, as shown in
136 Table 1.

137 **2.2 High-pressure cell and impedance measurements**

138 High-pressure complex impedance measurements for gabbroic melt were
139 performed by using Solartron-1260 impedance spectroscopy analyzer in the YJ-3000t
140 multi-anvil high-pressure apparatus. The cross-section diagram of sample assembly
141 for electrical conductivity measurements was shown in Fig. 1. Before high-pressure
142 cell was assembled, the cubic pressure medium of pyrophyllite with dimension of
143 $32.5 \times 32.5 \times 32.5 \text{ mm}^3$ and insulation sleeves were baked at 1073 K in a muffle furnace
144 for 5 hours to remove the absorbed water. The sample was placed at the middle of the
145 alumina and magnesia insulation sleeves, and sandwiched with two symmetric nickel
146 electrodes. The electrode was connected with a $\text{Ni}_{97}\text{Al}_3$ wire to a Solartron-1260
147 impedance spectroscopy analyzer. To shield against external electromagnetism and
148 spurious signal interference, the nickel foil with a thickness of 0.025 mm was installed
149 between the alumina and magnesia sleeves, and linked to the Earth line. Three-layer

150 stainless steel sheets with a total thickness of 0.5 mm were adopted as the heater, which
151 were installed between the cubic pressure medium of pyrophyllite and alumina sleeve.
152 After that, the sample assembly was stored in the vacuum dry furnace at 423 K for at
153 least 12 hours before the electrical conductivity measurements.

154 During the experiment, the pressure was slowly raised with a rate of 1.0 GPa h⁻¹
155 until it reached the desired value, and then the temperature was gradually increased with
156 a speed of 5.0 K min⁻¹. Under predesignated high-temperature and high-pressure
157 condition, impedance spectra of samples were collected in the frequency range of 10⁰–
158 10⁶ Hz and the applied signal voltage of 1.0 V. To obtain reproducible data, impedance
159 spectra of samples were measured at least two continuously heating-cooling cycles
160 under conditions of 873–1373 K and 1.0–3.0 GPa. The uncertainties of temperature and
161 pressure were less than 5.0 K and 0.1 GPa, respectively. The detailed experimental
162 principles and measurement procedures were described by Dai et al. (2008) and Hu et
163 al. (2022b).

164 **2.3 Determination of the water content**

165 The water content of gabbroic melt before and after the electrical conductivity
166 measurements was performed by virtue of the Vertex-70V and Hyperion-1000 vacuum
167 Fourier transform infrared (FT-IR) spectroscopy analyzer. The samples were double-
168 polished up to a thickness of ~50 μm. At least five spectra were conducted on the
169 different regions of transparent sample surfaces and made an average value in order to
170 avoid the heterogeneity effect of water distribution. A detailed experimental method
171 and procedure for the FT-IR measurement was detailedly presented by Hong et al.

172 (2022) and Hu et al. (2022b). For the hydrous gabbroic melts, the signal of the
 173 fundamental stretching H₂O vibrational spectroscopy at the peak position of ~3530
 174 cm⁻¹ revealed to be oversaturated, which was similar to the previously obtained results
 175 on hydrous dacitic melts reported by Laumonier et al. (2015). Two obviously
 176 characteristic peaks were appeared at two correspondent wavenumbers of ~4500 cm⁻¹
 177 and ~5200 cm⁻¹, which were representing the hydroxyl band and molecular water band
 178 of gabbroic melts, respectively (Stolper, 1982; Dixon et al., 1995). Hence, the peak area
 179 for the hydroxyl band and molecular water band was integrated to determine the water
 180 content of sample. The typical FT-IR spectra of gabbroic melt within the wavenumbers
 181 range of 2500–5800 cm⁻¹ are shown in Fig. 2. The water content of gabbroic melt (C_{melt})
 182 can be worked out by Beer-Lambert law,

$$183 \quad C = \omega A / \varepsilon \rho d \quad (1)$$

$$184 \quad C_{\text{melt}} = C_{\text{OH}} + C_{\text{H}_2\text{O}} \quad (2)$$

185 In here, the signal of ω stands for the molar mass of H₂O (18.02 g mole⁻¹), A stands for
 186 the integrated area of absorption spectra (cm⁻²), ρ stands for the density (g cm⁻³), d
 187 stands for the thickness of thin section (cm), and ε stands for the integral molar
 188 absorption coefficient (L mole⁻¹·cm⁻²). As presented the calculated melt density method
 189 by Luhr (2001), our density of gabbroic melt is determined as 2.764×10³ g L⁻¹. Molar
 190 absorption coefficients of ε_{OH} and $\varepsilon_{\text{H}_2\text{O}}$ were adopted from Dixon et al. (1995).
 191 According to the Eqs. 1 and 2, the water contents for three obtained hydrous gabbroic
 192 melts were calculated as 2.59 wt%, 5.92 wt% and 8.32 wt%, respectively. As displayed
 193 in Table 2, there is no significant loss of water for hydrous gabbroic melt during the

194 electrical conductivity experiment. At the same time, the corresponding error bars of
195 each water contents for the initial and recovered gabbroic melts are detailedly included
196 in Table 2.

197 **3 RESULTS**

198 In the present experiments, the electrical conductivity of gabbroic melt with four
199 different water contents (i.e. 0, 2.59 wt%, 5.92 wt% and 8.32 wt%) was measured at
200 temperature range of 873–1373 K and pressures of 1.0–3.0 GPa. The representative
201 complex impedance spectra of gabbroic melt with the 2.59 wt% water at conditions of
202 873–1373 K and 2.0 GPa were shown in Fig. 3. According to the theory of AC complex
203 impedance spectra, the impedance spectra of gabbroic melts within the high-frequency
204 range from $\sim 10^2$ – 10^3 Hz to 10^6 Hz can be interpreted as the bulk conduction mechanism
205 (i.e. grain interior), and whereas, the impedance spectra of sample within the low-
206 frequency range from 10^0 Hz to $\sim 10^2$ – 10^3 Hz represent the grain boundary conduction
207 mechanism or the polarization process at sample–electrode interface (Tyburczy and
208 Roberts (1990), Dai et al. (2008, 2012, 2013, 2014, 2016); Dai and Karato (2009a, b, c,
209 2020)). And thus, a series connection of R_S – CPE_S (R_S and CPE_S represent the resistance
210 and constant–phase element of the gabbroic melt, respectively) and R_E – CPE_E (R_E and
211 CPE_E represent the interface resistance and constant–phase element for electrode effect,
212 respectively) were employed as the equivalent circuit within a relatively lower
213 temperature range of 873–1123 K. As far as the higher temperature ranges of 1173–
214 1373 K, the equivalent circuit was consisted of the series connection of one resistance
215 and one parallel resistance with the constant phase element (CPE). The electrical

216 conductivity of sample can be calculated,

$$217 \quad \sigma = L/SR \quad (3)$$

218 In here, L , S and R stand for the length of sample (m), the cross-section area of electrode
219 (m^2) and the electrical resistance of sample (Ω), respectively. And the electrical
220 conductivity of gabbroic melt and temperatures conformed to the Arrhenius relation,

$$221 \quad \sigma = \sigma_0 \exp(-\Delta H/kT) \quad (4)$$

222 In here, σ_0 stands for the pre-exponential factor (S m^{-1}), k stands for the Boltzmann
223 constant (eV K^{-1}), and T stands for the absolute temperature (K), respectively. All of
224 these fitted parameters for the electrical conductivity of anhydrous and hydrous
225 gabbroic melt under conditions of 873–1373 K and 1.0–3.0 GPa were listed in Table 2.

226 For the gabbroic melt with a fixed water content of 2.59 wt%, the electrical
227 conductivity results for two continuously heating-cooling cycles at 873–1373 K and
228 3.0 GPa were shown in Fig. 4. In the first heating cycle within the temperature range of
229 923–1073 K, the electrical conductivity of sample was slightly deviated with those of
230 subsequent results in the first cooling and second heating-cooling cycles. Whereas, the
231 deviation degree became more and more small and finally overlapped at much higher
232 temperature range of 1123–1373 K. As a whole, the electrical conductivity of sample
233 was almost reproducible in the first cooling and second heating-cooling cycles. And
234 therefore, the electrical conductivity results were acquired by virtue of fitting
235 experimental data during the process of the first cooling and second heating-cooling
236 cycles.

237 4 Discussions

238 4.1 Influence of pressure on electrical conductivity

239 To identify the effect of pressure on the electrical conductivity of sample, the
240 electrical conductivity of hydrous gabbroic melt was acquired under condition of 873–
241 1373 K, 1.0–3.0 GPa and a fixed water content of 2.59 wt%. As illustrated in Fig. 5,
242 the electrical conductivity of sample and temperature conformed to the Arrhenius
243 relation at a certain water content and pressure condition. In the present studies, a
244 slightly negative dependence relation for the electrical conductivity of hydrous
245 gabbroic melt with a fixed water content of 2.59 wt% on the pressure was observed.
246 The electrical conductivity of sample slightly decreases by around 1.6 times at as
247 pressure enhances from 1.0 GPa to 3.0 GPa at temperature range of 873–1373 K.
248 Accordingly, the pre-exponential factor reduces from $3.02 \times 10^3 \text{ S m}^{-1}$ to $6.17 \times 10^2 \text{ S m}^{-1}$,
249 and the activation enthalpy value decreases from 0.85 eV to 0.81 eV, respectively.

250 Furthermore, the influence of pressure on the electrical conductivity of gabbroic
251 melt can be depicted as,

$$252 \quad \sigma = A_0(1-BP) \cdot \exp\left[-\frac{\Delta U + P\Delta V}{kT}\right] \quad (5)$$

253 In here, the pre-exponential factor (σ_0) and activation enthalpy (ΔH) of pressure
254 dependence can be illustrated as the relations of $\sigma_0 = A_0(1-BP)$ and $\Delta H = \Delta U + P\Delta V$. All
255 of the listed parameters including ΔU , ΔV , and P stand for the activation energy (eV),
256 the activation volume ($\text{cm}^3 \text{ mole}^{-1}$) and pressure (GPa), and as well as B is representing
257 a constant, respectively. Furthermore, the electrical conductivity of gabbroic melt along
258 with the variations of temperature, pressure and water content is fitted accordingly and

259 the detailed fitting results are displayed in Table 3. The logarithmic electrical
260 conductivity of gabbroic melt with a fixed water content of 2.59 wt% and the inverse
261 temperature follows a good linear relation, which reveals only one main conduction
262 mechanism operating the electrical transport within our experimental temperature and
263 pressure ranges. By virtue of the available pressure–dependent electrical conductivity,
264 we also can extrapolate the relationship between the electrical conductivity of gabbroic
265 melt with a fixed water content of 2.59 wt% and temperature at atmospheric pressure.
266 And then the pre–exponential factor and activation enthalpy at room pressure are
267 calculated as 5177 S m^{-1} and 0.87 eV, respectively. According to Eq. 5 and Table 3, the
268 activation energy and activation volume of gabbroic melt with a fixed water content of
269 2.59 wt% can be determined as $0.87 \pm 0.04 \text{ eV}$ and $-1.98 \pm 0.52 \text{ cm}^3 \text{ mole}^{-1}$.

270 **4.2 Influence of water content on electrical conductivity**

271 For a fixed pressure of 1.0 GPa, the influence of water content on the electrical
272 conductivity of gabbroic melt at temperature range of 873–1373 K is detailedly shown
273 in Fig. 6. The electrical conductivity of gabbroic melt with four different water contents
274 gradually increases with the rise of temperature. For each correspondent water content
275 (i.e. 0, 2.59 wt%, 5.92 wt% and 8.32 wt%), the logarithm of electrical conductivity of
276 the sample and reciprocal temperature follows a good linear relation. On the other hand,
277 when water content of gabbroic melt enhances from 0 to 8.32 wt%, the electrical
278 conductivity of gabbroic melts tends to visibly increase, and whereas the activation
279 enthalpy gradually reduces from 0.93 eV to 0.63 eV, accordingly. In short, our presently
280 acquired electrical conductivity results show a substantial enhancement of water on the

281 electrical conductivity of gabbroic melt, which are also observed among the electrical
282 conductivity of other representative calc–alkaline igneous rock melts in the recent years
283 (Ni et al., 2011; Laumonier et al., 2015; Guo et al., 2017; Chen et al., 2018).

284 The electrical conductivity of hydrous gabbroic melt can be expressed in terms of
285 the charge species concentration dependence of the pre–exponential factor (A), which
286 behaves in an Arrhenius relation,

$$287 \quad \sigma = (A_1 + A_2 \cdot C_w^r) \cdot \exp\left(\frac{-\Delta H_0 - \alpha C_w^\beta}{RT}\right) \quad (6)$$

288 In here, C_w is water content of the sample (wt%), ΔH_0 stands for the activation enthalpy,
289 and α , β and r stand for empirical power–law constants. By a non–linear global least–
290 squares method, the electrical conductivity of gabbroic melt with different water
291 contents was fitted and the fitted parameter results were listed in Table 4. For the
292 magnitude of water–dependent relation of r (0.43 ± 0.05), it makes clear that the water
293 can dramatically enhance the electrical conductivity of gabbroic melt at conditions of
294 873–1373 K and 1.0 GPa.

295 **4.3 Comparisons with previous studies**

296 As displayed in Fig. 7, five previously reported results on the electrical
297 conductivity of natural gabbro samples were employed to compare with our absolutely
298 new results for the electrical conductivity of gabbroic melt (Sato and Ida, 1984;
299 Schilling et al., 1997; Maumus et al., 2005; Dai et al., 2015; Saito and Bagdassarov,
300 2018). As a whole, our acquired electrical conductivity results on gabbroic melts are
301 obviously higher than those of natural gabbro at temperature range of 873–1373 K and
302 pressure of 1.0 GPa. Both Sato and Ida (1984) and Schilling et al. (1997) have already

303 performed the electrical conductivity measurements on natural gabbro at high
304 temperature and atmospheric pressure. In case of the occurrence of temperature–
305 induced partial melting, the electrical conductivity of sample will be increased rapidly
306 by several orders of magnitude. However, we find that there is no any relevant
307 information on the water content for their previously reported electrical conductivity
308 results on those of listed melting–bearing natural gabbro samples. The electrical
309 conductivity results of natural gabbro containing 34 vol% melt from Maumus et al.
310 (2005) are much lower than those of our present gabbroic melt, and the obvious
311 discrepancy is possibly caused from the differentiation of the chemical composition and
312 water content of gabbroic melt. In comparison with Saito and Bagdassarov (2018), there
313 is a jump of three orders of magnitude in the electrical conductivity of sample, which
314 is possibly originated from a relatively larger influence of melt volume percentage. As
315 far as the previously reported electrical conductivity of natural gabbro with a relatively
316 lower water content of ~610 ppm and free of any melt by Dai et al. (2015) at pressures
317 of 0.5–2.0 GPa, there is an approximate electrical conductivity result on the anhydrous
318 gabbroic melt to be observed in the present studies. And however, the dependence of
319 electrical conductivity of anhydrous and hydrous gabbroic melts on the temperature,
320 pressure and water content is still scarce under high–temperature and high–pressure
321 conditions until now.

322 It is well known that the gabbroic melt is belonging to one type of representative
323 calc–alkaline igneous rock. As usual, previously available conductivity results
324 confirmed that the electrical conductivity of calc–alkaline igneous rock melts (i.e.

325 dacitic melt, andesitic melt and basaltic melt) is also highly sensitive to the influential
326 factor of the degree of depolymerization at high temperature and high pressure (Ni et
327 al., 2011; Laumonier et al., 2015; Guo et al., 2017). The degree of depolymerization
328 can be characterized by the ratio of non-bridging oxygen ions per tetrahedrally
329 coordinated cation (NBO/T). As pointed out by Mysen et al. (1982), the magnitude of
330 degree of depolymerization on gabbroic melt can be worked out by our above-
331 mentioned EPMA results in Table 1. And the dependence relation of electrical
332 conductivity of gabbroic melts and degree of depolymerization was clearly displayed
333 in Fig. 8 under conditions of four different water contents (i.e. 0, 2.59 wt%, 5.92 wt%
334 and 8.32 wt%), 1373 K and 1.0 GPa. Under constant degree of depolymerization, it
335 makes clear that a relatively lower electrical conductivity is observed in the anhydrous
336 gabbroic melt under condition of 1373 K and 1.0 GPa. With the rise of water content,
337 the electrical conductivity of gabbroic melts dramatically increases, whereas the
338 variation degree for the electrical conductivity gradually reduces. At the same time, we
339 also compared the presently obtained electrical conductivity results for anhydrous and
340 hydrous gabbroic melts with other three representative calc-alkaline igneous melts
341 reported by Ni et al. (2011), Laumonier et al. (2015) and Guo et al. (2017), as detailedly
342 illustrated in Fig. 8. On the base of the previously calculating method for the degree of
343 depolymerization (NBO/T) of melt transforming the detailed EPMA data, the
344 magnitudes in the degree of depolymerization for our present gabbroic melt and other
345 three representative calc-alkaline igneous rock melts (i.e. dacitic melt, andesitic melt
346 and basaltic melt) are 0.65, 0.07, 0.35 and 0.81, respectively. As a whole, the electrical

347 conductivity of four typical calc–alkaline igneous rock melts will increase with the rise
348 of the degree of depolymerization at a fixed water content. As the water content will be
349 enhanced from 0 to 8.32 wt%, the electrical conductivity of each calc–alkaline igneous
350 rock melts will dramatically increase. It is obviously observed that the correspondent
351 variations in the electrical conductivity of calc–alkaline igneous rock melts along the
352 orders from dacitic melt to andesitic melt to gabbroic melt to basaltic melt tend to
353 gradually reduce, and become more and more convergent, accordingly. To my best
354 knowledge, the magnitude in the degree of depolymerization (NBO/T) for the melt
355 sample is highly positive relation with the content variations of alkali–bearing and alkali
356 earth–bearing cations (i.e. Na⁺, K⁺, Ca²⁺, Mg²⁺, etc.) (Mysen et al., 1982; Lee et al.,
357 2003; Di Genova et al., 2015). Just as presented the EPMA results, the total contents of
358 alkali cations and alkali–earth cations are determined as the 11.54 wt% of dacitic melt
359 reported by Laumonier et al. (2015), the 20.41 wt% of andesitic melt reported by Guo
360 et al. (2017), the 30.23 wt% of basaltic melt reported by Ni et al. (2011), and as well as
361 the 25.53 wt% of gabbroic melt in this study. And thus, the degree of depolymerization
362 for the calc–alkaline igneous rock melts along the orders from dacitic melt to andesitic
363 melt to gabbroic melt to basaltic melt will gradually increase, accordingly. On the other
364 hand, previous electrical conductivity results have confirmed that the main charge
365 carriers of the calc–alkaline igneous melts are alkali cations and alkali–earth cations at
366 high temperature and high pressure (Ni et al., 2011; Laumonier et al., 2015; Guo et al.,
367 2017; Chen et al., 2018). And thus, the influence of the degree of depolymerization on
368 the electrical conductivity of melt is possibly caused from the concentration of the alkali

369 cations and alkali–earth cations. Accordingly, the electrical conductivity of calc–
370 alkaline igneous melts will gradually increase with the rise of alkali cations and alkali–
371 earth cations along the orders from dacitic melt to andesitic melt to gabbroic melt to
372 basaltic melt. In sum, as followed the orders from dacitic melt to andesitic melt to
373 gabbroic melt to basaltic melt, it is very reasonable that the electrical conductivity of
374 calc–alkaline igneous melts will be gradually enhanced with the rise of degree of
375 depolymerization (NBO/T) under conditions of 1373 K and 1.0 GPa.

376 **5 Geophysical implications**

377 As a typical active plate geotectonic boundary, previously available
378 magnetotelluric results have already revealed that the phenomenon of high conductivity
379 anomalies is widespread distributed in the region of mid–ocean ridge (Key et al., 2013;
380 Miensopust et al., 2014). For the representative Mohns ridge of the Arctic Ocean, there
381 widely exist a large number of high conductive layers with their conductivity magnitude
382 within the range of $\sim 0.08\text{--}0.32\text{ S m}^{-1}$ at the correspondent depths from 4 km to 7 km
383 (Johansen et al., 2019). All of these acquired seismic and gravitational survey datasets
384 have confirmed that various volume percentages of gabbroic melt widely outcropped
385 in the Mohns ridge of the Arctic Ocean at the depths of $\sim 4\text{--}11$ km (Géli et al., 1994;
386 Conley and Dunn, 2011). And therefore, the high conductivity anomalies in the Mohns
387 ridge of the Arctic Ocean are possibly correlated with the gabbroic melt at high
388 temperature and high pressure. In conjunction with our presently obtained experimental
389 results on the electrical conductivity of anhydrous and hydrous gabbroic melts at
390 conditions of 873–1373 K and 1.0–3.0 GPa, the typical Hashin–Shtrikman upper bound

391 model and previously available magnetotelluric results, the electrical conductivity of
 392 gabbroic melt–olivine system was constructed in detail, as displayed in Fig. 9. All of
 393 these influential ingredients including water content and volume percentage were
 394 comprehensively considered. During the process of the expansion of mid–ocean ridge
 395 caused by the rapid upwelling of asthenosphere mantle, the geothermal distribution
 396 exhibited an abnormal behavior in the Mohns ridge of the Arctic Ocean. As pointed out
 397 by Johansen et al. (2019), the temperature on the top gabbro layer is approximate to
 398 1373 K along the ultraslow–spreading Arctic mid–ocean Mohns ridge region. In
 399 addition, the effect of pressure on the electrical conductivity of gabbroic melt is rather
 400 feeble, and it can be neglected.

401 For the representative Mohns ridge of the Arctic Ocean, previously available
 402 petrological and geochemical results have already revealed that the range of water
 403 content for the crustal rock and melt in the Mohns ridge is ~0.25–2.64 wt% (Neumann
 404 and Schilling, 1984; Poreda et al., 1986). The electrical conductivity results of gabbroic
 405 melt with two different water contents (anhydrous and a water content of 2.59 wt%) are
 406 selected from our present studies. The electrical conductivity of olivine at 1373 K and
 407 1.0 GPa is properly extrapolated from the available experimental data of polycrystalline
 408 olivine under conditions of 160 ppm wt water content, 873–1273 K and 4.0–10.0 GPa
 409 reported by Dai and Karato (2014). On the variation of volume percentage for the
 410 gabbroic melt, the electrical conductivity of a gabbroic melt–olivine system (σ_{HS+}) can
 411 be expressed as (Hashin and Shtrikman, 1962),

$$412 \quad \sigma_{HS+} = \sigma_{melt} + [(1-X_{melt}) \cdot (\sigma_{olivine} - \sigma_{melt})^{-1} + X_{melt} / (3 \cdot \sigma_{melt})]^{-1} \quad (7)$$

413 In here, the signals of σ_{melt} and σ_{olivine} stand for the electrical conductivity of gabbroic
414 melt from the present study and that of polycrystalline olivine with a certain water
415 content of 160 ppm wt from Dai and Karato (2014), respectively; X_{melt} stands for the
416 volume percentage of gabbroic melt.

417 The electrical conductivity of gabbroic melt–olivine system with different volume
418 percentage of gabbroic melt was successfully worked out at 1373 K and 1.0 GPa, as
419 displayed in Fig. 9. For the gabbroic melt–olivine system with a certain volume
420 percentage of gabbroic melt, the electrical conductivity increases with the rise of water
421 content in gabbroic melt. As far as the gabbroic melt containing a fixed water content,
422 the electrical conductivity of gabbroic melt–olivine system gradually enhances as the
423 volume percentage of gabbroic melt increases. As pointed out by Johansen et al. (2019),
424 the range of electrical conductivity for the HCL in the Mohns ridge is $\sim 0.08\text{--}0.32 \text{ S m}^{-1}$,
425 as displayed in the orange region of Fig. 9. For the anhydrous gabbroic melt, the
426 required volume percentage for the high conductivity anomalies the ultraslow-
427 spreading Arctic mid-ocean Mohns ridge region falls within the range of $\sim 2.93\text{--}34.69$
428 vol%, which is in good agreement with previously inferred results from geophysical
429 observations (Géli et al., 1994; Conley and Dunn, 2011). When the water content of
430 gabbroic melt increases, the required volume percentage for the HCL reduces
431 accordingly. As for the gabbroic melt with a relatively high water content of 2.59 wt%,
432 its volume percentage range of $\sim 2.63\text{--}23.63$ vol% is enough to explain the high
433 conductivity anomalies. In summary, the high conductivity anomalies in the Mohns
434 ridge of the Arctic Ocean could be interpreted by the anhydrous and hydrous gabbroic

435 melt, and our present electrical conductivity results for gabbroic melt with different
436 water contents can provide an important constraint for the water content and volume
437 percentage of gabbroic melt at depth range of ~4–7 km within the Mohns ridge region
438 of the Arctic Ocean.

439 **Conclusions**

440 In the present studies, the electrical conductivity of gabbroic melt with different
441 water contents of 0–8.32 wt% were measured at temperatures of 873–1373 K and
442 pressures of 1.0–3.0 GPa. For the gabbroic melt with a fixed water content of 2.59 wt%,
443 the electrical conductivity of the sample decreases slightly with the rise of pressure, and
444 its corresponding activation energy and activation volume are determined as 0.87 ± 0.04
445 eV and $-1.98 \pm 0.02 \text{ cm}^3 \text{ mole}^{-1}$, respectively. When water content of gabbroic melt
446 enhances from 0 to 8.32 wt% under the certain conditions of 873–1373 K and 1.0 GPa,
447 the electrical conductivity of gabbroic melts tends to visibly increase, and whereas the
448 activation enthalpy gradually reduces from 0.93 eV to 0.63 eV, accordingly.
449 Furthermore, the functional relation models for the electrical conductivity of gabbroic
450 melt with the variations of temperature, pressure and water content are constructed at
451 high-temperature and high-pressure conditions, respectively. By virtue of typical
452 Hashin–Shtrikman upper bound model, the electrical conductivity of gabbroic melt–
453 olivine system on the variation of melt volume percentage is calculated under the
454 conditions of four different water contents of gabbroic melt (i.e. 0, 2.59 wt%, 5.92 wt%
455 and 8.32 wt%), 1373 K and 1.0 GPa, which can be employed to reasonably explain the

456 high conductivity anomalies in the Mohns ridge of the Arctic Ocean observed by the
457 previously available field MT results.

458 *Data availability.* The data that support the findings of this study are available from
459 the first author upon reasonable request.

460 *Acknowledgements.* We thank the editor of Professor Yang Chu from Institute of
461 Geology and Geophysics, Chinese Academy of Sciences, and two anonymous
462 reviewers for their very constructive and enlightened comments and suggestions in the
463 reviewing process, which helped us greatly in improving the manuscript. This research
464 was financially supported by the NSF of China (grant number 42072055 and 42274137)
465 and the Youth Innovation Promotion Association of CAS (grant number 2019390).

466 *Declaration of competing interest.* The authors declare that they have no conflict
467 of interest.

468 **References**

- 469 Almeev, R., Holtz, F., Koepke, J., Haase, K., and Devey, C.: Depths of partial
470 crystallization of H₂O-bearing MORB: Phase equilibria simulations of basalts at
471 the MAR near Ascension Island (7–11°S), *J. Petrol.*, 49, 25–45, 2008.
- 472 Chen, J. Y., Gaillard, F., Villaros, A., Yang, X. S., Laumonier, M., Jolivet, L., Unsworth,
473 M., Hashim, L., Scaillet, B., and Richard, G.: Melting conditions in the modern
474 Tibetan crust since the Miocene, *Nat. Commun.*, 9, 3515,
475 <https://doi.org/10.1038/s41467-018-05934-7>, 2018.
- 476 Conley, M. M. and Dunn, R. A.: Seismic shear wave structure of the uppermost mantle
477 beneath the Mohns Ridge, *Geochem. Geophys. Geosyst.*, 12, Q0AK01,
478 <https://doi.org/10.1029/2011GC003792>, 2011.
- 479 Dai, L. D., Li, H. P., Hu, H. Y., and Shan, S. M.: Experimental study of grain boundary
480 electrical conductivities of dry synthetic peridotite under high-temperature, high-
481 pressure, and different oxygen fugacity conditions, *J. Geophys. Res. Solid Earth*,
482 113, B12211, <https://doi.org/10.1029/2008JB005820>, 2008.
- 483 Dai, L. D. and Karato, S. I.: Electrical conductivity of pyrope-rich garnet at high
484 temperature and high pressure, *Phys. Earth Planet. Inter.*, 176, 83–88, 2009a.
- 485 Dai, L. D. and Karato, S. I.: Electrical conductivity of orthopyroxene: Implications for
486 the water content of the asthenosphere, *Proc. Jpn. Acad. Ser. B*, 85, 466–475,
487 2009b.
- 488 Dai, L. D. and Karato, S. I.: Electrical conductivity of wadsleyite at high temperatures
489 and high pressures, *Earth Planet. Sci. Lett.*, 287, 277–283, 2009c.

490 Dai, L. D., Li, H. P., Hu, H. Y., Shan, S. M., Jiang, J. J., and Hui, K. S.: The effect of
491 chemical composition and oxygen fugacity on the electrical conductivity of dry
492 and hydrous garnet at high temperatures and pressures, *Contrib. Mineral. Petrol.*,
493 163, 689–700, 2012.

494 Dai, L. D., Li, H. P., Hu, H. Y., Jiang, J. J., Hui, K. S., and Shan, S. M.: Electrical
495 conductivity of $\text{Alm}_{82}\text{Py}_{15}\text{Grs}_3$ almandine-rich garnet determined by impedance
496 spectroscopy at high temperatures and high pressures, *Tectonophysics*, 608, 1086–
497 1093, 2013.

498 Dai, L. D., Hu, H. Y., Li, H. P., Jiang, J. J., and Hui, K. S.: Effects of temperature,
499 pressure and chemical composition on the electrical conductivity of granite and its
500 geophysical implications, *Am. Mineral.*, 99, 1420–1428, 2014.

501 Dai, L. D. and Karato, S. I.: The effect of pressure on the electrical conductivity of
502 olivine under the hydrogen-rich conditions, *Phys. Earth Planet. Inter.*, 232, 51–56,
503 2014.

504 Dai, L. D., Hu, H. Y., Li, H. P., Hui, K. S., Jiang, J. J., Li, J., and Sun, W. Q.: Electrical
505 conductivity of gabbro: The effects of temperature, pressure and oxygen fugacity,
506 *Eur. J. Mineral.*, 27, 215–224, 2015.

507 Dai, L. D., Hu, H. Y., Li, H. P., Wu, L., Hui, K. S., Jiang J. J., and Sun, W. Q.: Influence
508 of temperature, pressure, and oxygen fugacity on the electrical conductivity of dry
509 eclogite, and geophysical implications, *Geochem. Geophys. Geosyst.*, 17, 2394–
510 2407, 2016.

511 Dai, L. D. and Karato, S. I.: Electrical conductivity of Ti-bearing hydrous olivine

512 aggregates at high temperature and high pressure, *J. Geophys. Res. Solid Earth*,
513 125, e2020JB020309, <https://doi.org/10.1029/2020JB020309>, 2020.

514 Di Genova, D., Morgavi, D., Hess, K. U., Neuville, D. R., Borovkov, N., Perugini, D.,
515 and Dingwell, D. B.: Approximate chemical analysis of volcanic glasses using
516 Raman spectroscopy, *J. Raman Spectrosc.*, 46, 1235–1244, 2015.

517 Dixon, J. B., Stolper, E. M., and Holloway, J. R.: An experimental study of water and
518 carbon dioxide solubilities in mid-ocean ridge basaltic liquids. Part I: Calibration
519 and solubility models, *J. Petrol.*, 36, 1607–1631, 1995.

520 Förster, M. W. and Selway, K.: Melting of subducted sediments reconciles geophysical
521 images of subduction zones, *Nat. Commun.*, 12, 1320,
522 <https://doi.org/10.1038/s41467-021-21657-8>, 2021.

523 Géli, L., Renard, V., and Rommevaux, C.: Ocean crust formation processes at very slow
524 spreading centers: A model for the Mohns Ridge, near 72°N, based on magnetic,
525 gravity, and seismic data, *J. Geophys. Res. Solid Earth*, 99, 2995–3013, 1994.

526 Guo, X., Li, B., Ni, H. W., and Mao, Z.: Electrical conductivity of hydrous andesitic
527 melts pertinent to subduction zones, *J. Geophys. Res. Solid Earth*, 122, 1777–1788,
528 2017.

529 Hashin, Z. and Shtrikman, S.: A variation approach to the theory of effective magnetic
530 permeability of multiphase materials, *J. Appl. Phys.*, 33, 3125–3131, 1962.

531 Hong, M. L., Dai, L. D., Hu, H. Y., Yang, L. F. and Zhang, X. Y.: Pressure-induced
532 structural phase transitions in natural kaolinite investigated by Raman
533 spectroscopy and electrical conductivity, *Am. Mineral.*, 107, 385–394, 2022.

534 Hu, H. Y., Dai, L. D., Sun, W. Q., Wang, M. Q., and Jing, C. X.: Constraints on fluids
535 in the continental crust from laboratory-based electrical conductivity
536 measurements of plagioclase, *Gondwana Res.*, 107, 1–12, 2022a.

537 Hu, H. Y., Jing, C. X., Dai, L. D., Yin, C. Y. and Chen, D. M.: Electrical conductivity
538 of siderite and its implication for high conductivity anomaly in the slab-mantle
539 wedge interface, *Front. Earth Sci.*, 10, 985740,
540 <https://doi.org/10.3389/feart.2022.985740>, 2022b.

541 Johansen, S. E., Panzner, M., Mittet, R., Amundsen, H. E. F., Lim, I., Vik, E., Landrø,
542 M., and Arntsen, B.: Deep electrical imaging of the ultraslow-spreading Mohns
543 ridge, *Nature*, 567, 379–383, 2019.

544 Key, K., Constable, S., Liu, L. J., and Pommier, A.: Electrical image of passive mantle
545 upwelling beneath the northern East Pacific Rise, *Nature*, 495, 499–502, 2013.

546 Laumonier, M., Gaillard, F., and Sifre, D.: The effect of pressure and water
547 concentration on the electrical conductivity of dacitic melts: Implication for
548 magnetotelluric imaging in subduction areas, *Chem. Geol.*, 418, 66–76, 2015.

549 Lee, S. K., Mysen, B. O., and Cody, G. D.: Chemical order in mixed-cation silicate
550 glasses and melts, *Phys. Rev. B*, 68, 214206,
551 <https://doi.org/10.1103/PhysRevB.68.214206>, 2003.

552 Leuthold, J., Lissenberg, C. J., O’Driscoll, B., Karakas, O., Falloon, T., Klimentyeva,
553 D. N., and Ulmer, P.: Partial melting of lower oceanic crust gabbro: Constraints
554 from poikilitic clinopyroxene primocrysts, *Front. Earth Sci.*, 6, 15,
555 <https://doi.org/10.3389/feart.2018.00015>, 2018.

556 Li, G. H., Gao, Y., Zhou, Y. Z., Ju, C. H., Shi, Y. T., and Cui, Q. H.: A low-velocity
557 layer atop the mantle transition zone beneath the western Central Asian Orogenic
558 Belt: Upper mantle melting induced by ancient slab subduction, *Earth Planet. Sci.*
559 *Lett.*, 578, 117287, <https://doi.org/10.1016/j.epsl.2021.117287>, 2022.

560 Luhr, J. F.: Glass inclusions and melt volatile contents at Parícutin Volcano, Mexico,
561 *Contrib. Mineral. Petrol.*, 142, 261–283, 2001.

562 Maumus, J., Bagdassarov, N., and Schmeling, H.: Electrical conductivity and partial
563 melting of mafic rocks under pressure, *Geochim. Cosmochim. Ac.*, 69, 4703–4718,
564 2005.

565 Miensopust, M. P., Jones, A. G., Hersir, G. P., and Vilhjálmsson, A. M.: The
566 Eyjafjallajökull volcanic system, Iceland: Insights from electromagnetic
567 measurements, *Geophys. J. Int.*, 199, 1187–1204, 2014.

568 Mysen, B. O., Virgo, D., and Seifert, F. A.: The structure of silicate melts: Implications
569 for chemical and physical properties of natural magma, *Rev. Geophys.*, 20, 353–
570 383, 1982.

571 Neumann, E. R. and Schilling, J. G.: Petrology of basalts from the Mohns–Knipovich
572 Ridge; the Norwegian–Greenland Sea, *Contrib. Mineral. Petrol.*, 85, 209–223,
573 1984.

574 Ni, H. W., Keppler, H., and Behrens, H.: Electrical conductivity of hydrous basaltic
575 melts: Implications for partial melting in the upper mantle, *Contrib. Mineral.*
576 *Petrol.*, 162, 637–650, 2011.

577 Poreda, R., Schilling, J. G., and Craig, H.: Helium and hydrogen isotopes in ocean–

578 ridge basalts north and south of Iceland, *Earth Planet. Sci. Lett.*, 78, 1–17, 1986.

579 Saito, S. and Bagdassarov, N. S.: Laboratory measurements of electrical conductivity in
580 a gabbro of the Oman ophiolite at high–pressures and high–temperatures:
581 Implications for interpretation of resistivity structures of lower oceanic crust, *J.*
582 *Mineral. Petrol. Sci.*, 113, 112–117, 2018.

583 Sato, H. and Ida, Y.: Low frequency electrical impedance of partially molten gabbro:
584 the effect of melt geometry on electrical properties, *Tectonophysics*, 107, 105–134,
585 1984.

586 Schilling, F. R., Partzsch, G. M., Brasse, H., and Schwarz, G.: Partial melting below the
587 magmatic arc in the central Andes deduced from geoelectromagnetic field
588 experiments and laboratory data, *Phys. Earth Planet. Inter.*, 103, 17–31, 1997.

589 Shaw, A. M., Behn, M. D., Humphris, S. E., Sohn, R. A., and Gregg, P. M.: Deep
590 pooling of low degree melts and volatile fluxes at the 85°E segment of the Gakkel
591 Ridge: Evidence from olivine-hosted melt inclusions and glasses, *Earth Planet. Sci.*
592 *Lett.*, 289, 311–322, 2010.

593 Shen, Y. and Forsyth, D. W.: Geochemical constraints on initial and final depths of
594 melting beneath mid-ocean ridges, *J. Geophys. Res. Solid Earth*, 100, 2211–2237,
595 1995.

596 Sim, S. J., Spiegelman, M., Stegman, D. R., and Wilson, C.: The influence of spreading
597 rate and permeability on melt focusing beneath mid-ocean ridges, *Phys. Earth*
598 *Planet. Inter.*, 304, 106486, <https://doi.org/10.1016/j.pepi.2020.106486>, 2020.

599 Stolper, E.: The speciation of water in silicate melts, *Geochim. Cosmochim. Ac.*, 46,

600 2609–2620, 1982.

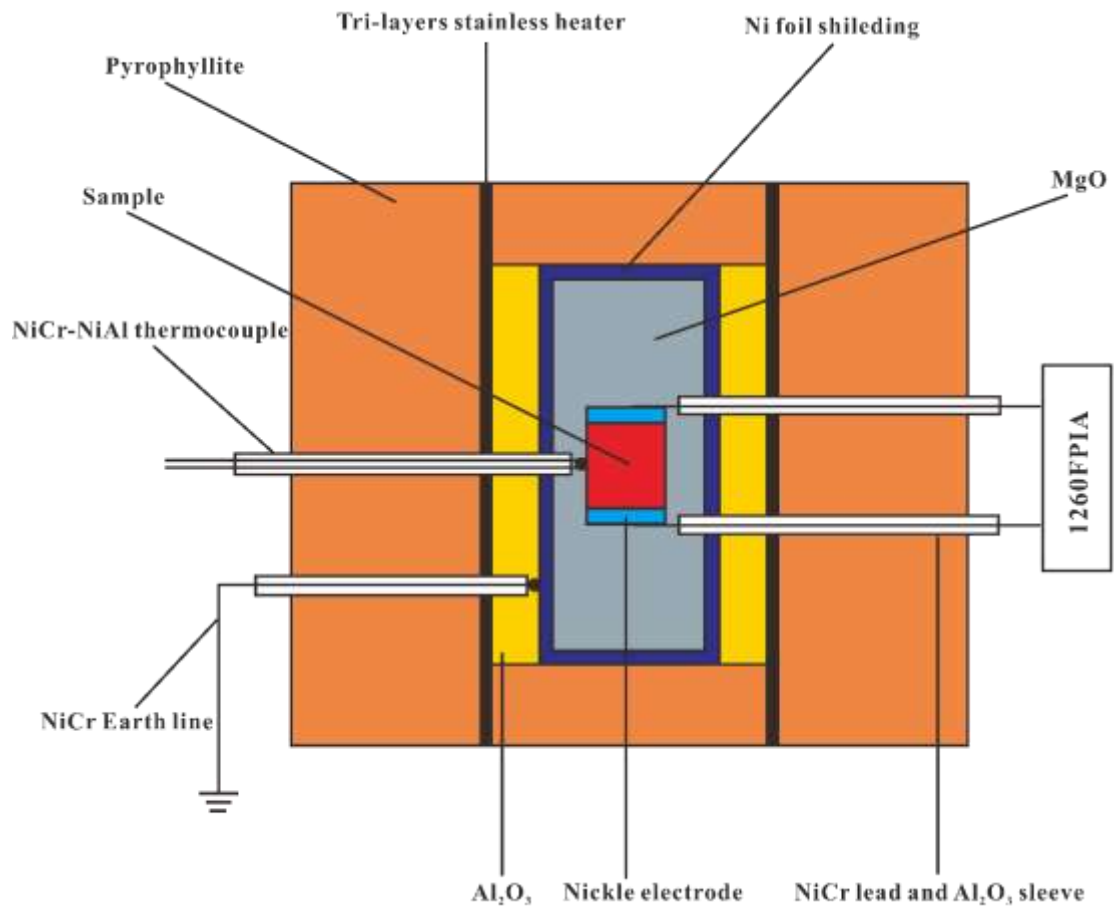
601 Turner, S. J. and Langmuir, C. H.: Sediment and ocean crust both melt at subduction
602 zones, *Earth Planet. Sci. Lett.*, 584, 117424,
603 <https://doi.org/10.1016/j.epsl.2022.117424>, 2022.

604 Tyburczy, J. A. and Roberts, J. J.: Low frequency electrical response of polycrystalline
605 olivine compacts: Grain boundary transport, *Geophys. Res. Lett.*, 17, 1985–1988,
606 1990.

607 Wallace, P. J.: Volatiles in subduction zone magmas: concentrations and fluxes based
608 on melt inclusion and volcanic gas data, *J. Volcanol. Geoth. Res.*, 140, 217–240,
609 2005.

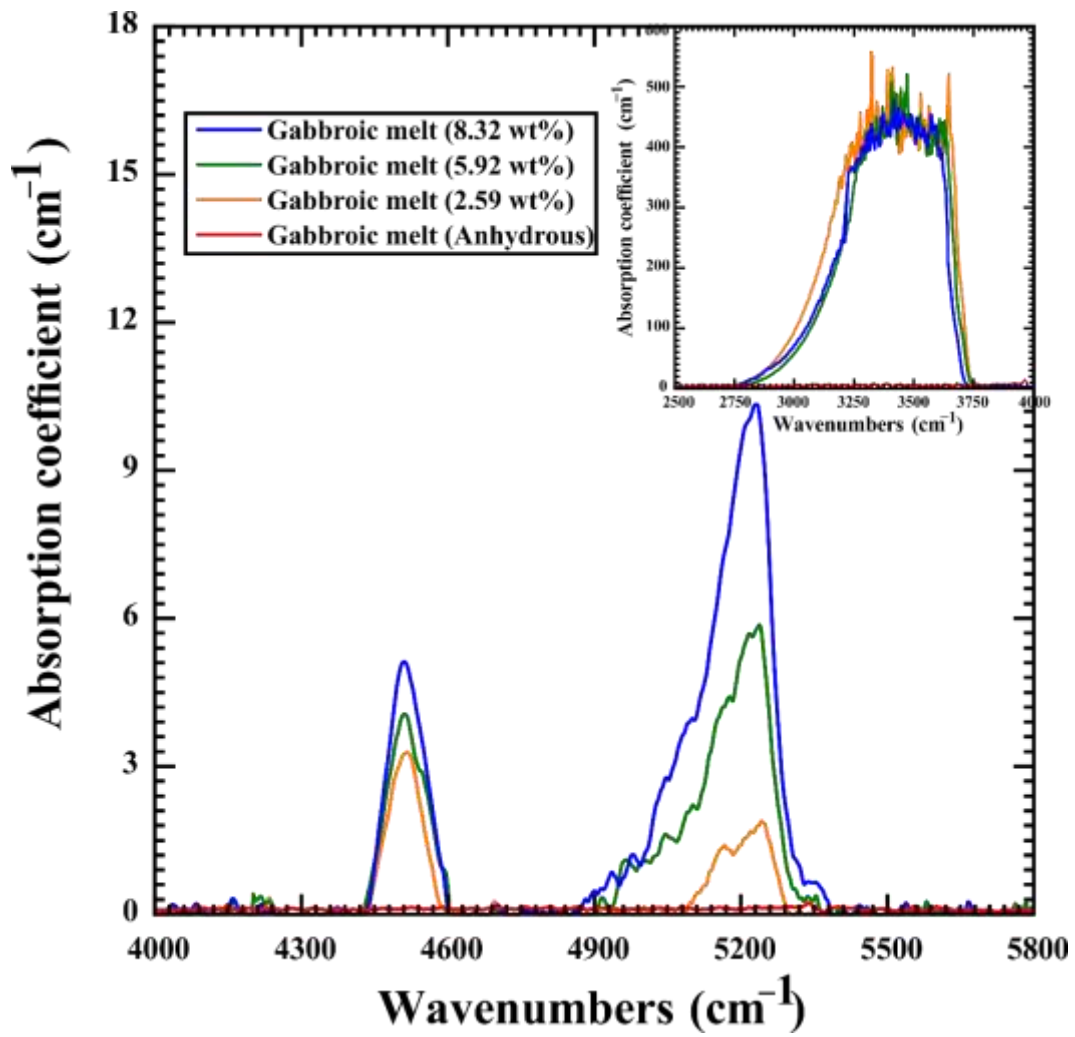
610 White, R. S., Minshull, T.A., Bickle, M. J., and Robinson, C. J.: Melt generation at very
611 slow-spreading oceanic ridges: Constraints from geochemical and geophysical
612 data, *J. Petrol.*, 42, 1171–1196, 2001.

613 Wu, K., Ling, M. X., Hu, Y. B., Guo, J., Jiang, X. Y., Sun, S. J., Liang, H. Y., Liu, X.,
614 and Sun, W. D.: Melt-fluxed melting of the heterogeneously mixed lower arc crust:
615 A case study from the Qinling orogenic belt, Central China, *Geochem. Geophys.*
616 *Geosyst.*, 19, 1767–1788, 2018.



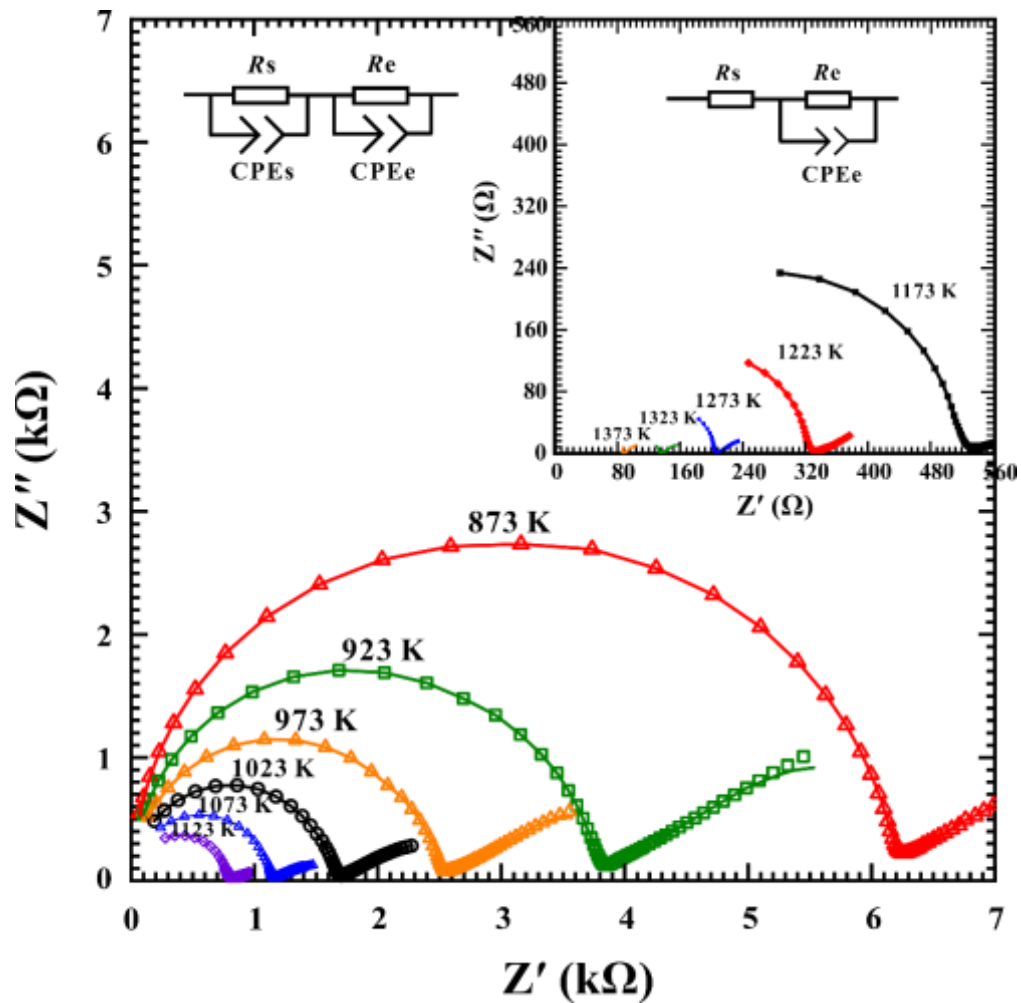
617

618 **Figure 1.** The experimental setup for the electrical conductivity measurements of
 619 gabbroic melt at high temperatures and high pressures.



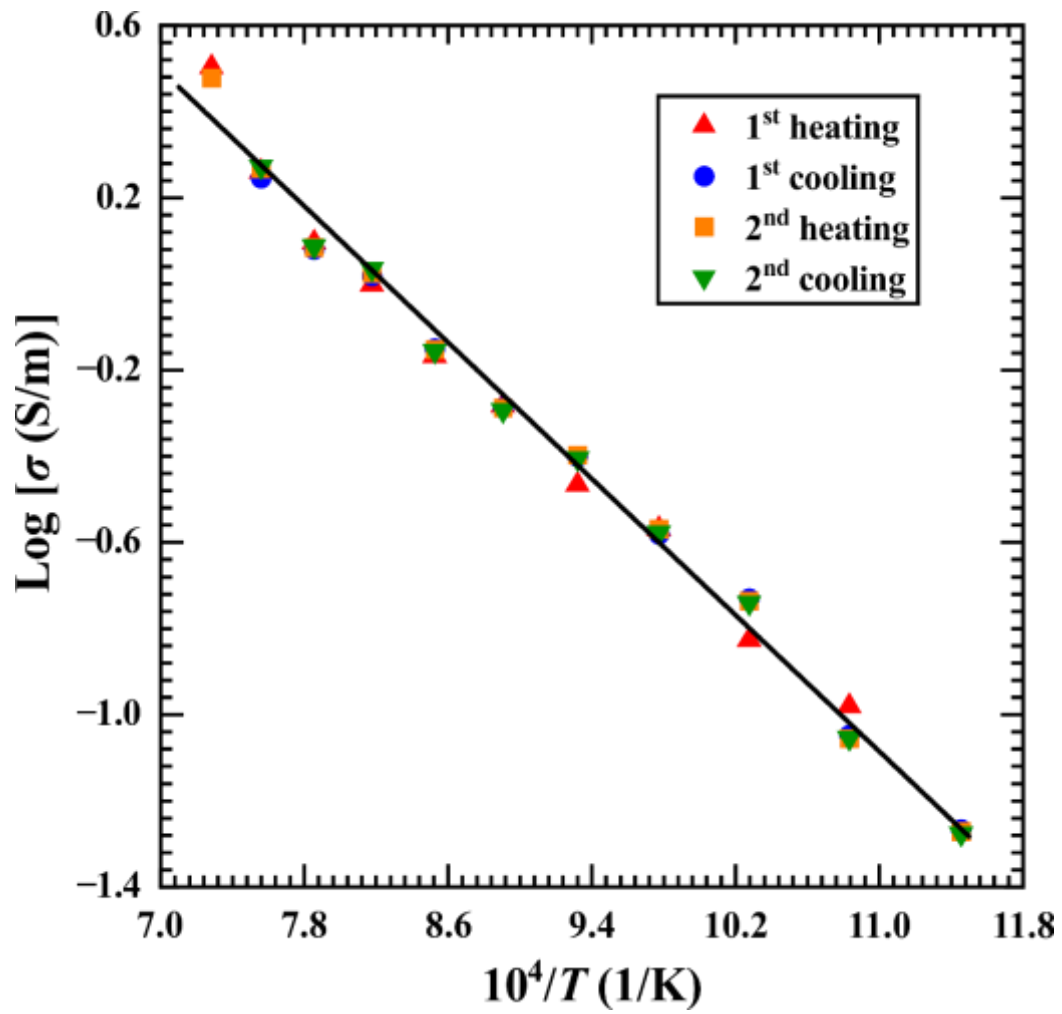
620

621 **Figure 2.** The representative FT-IR spectra of the gabbroic melt with various water
 622 contents in the wavenumbers range of 4000–5800 cm⁻¹ and 2500–4000 cm⁻¹.



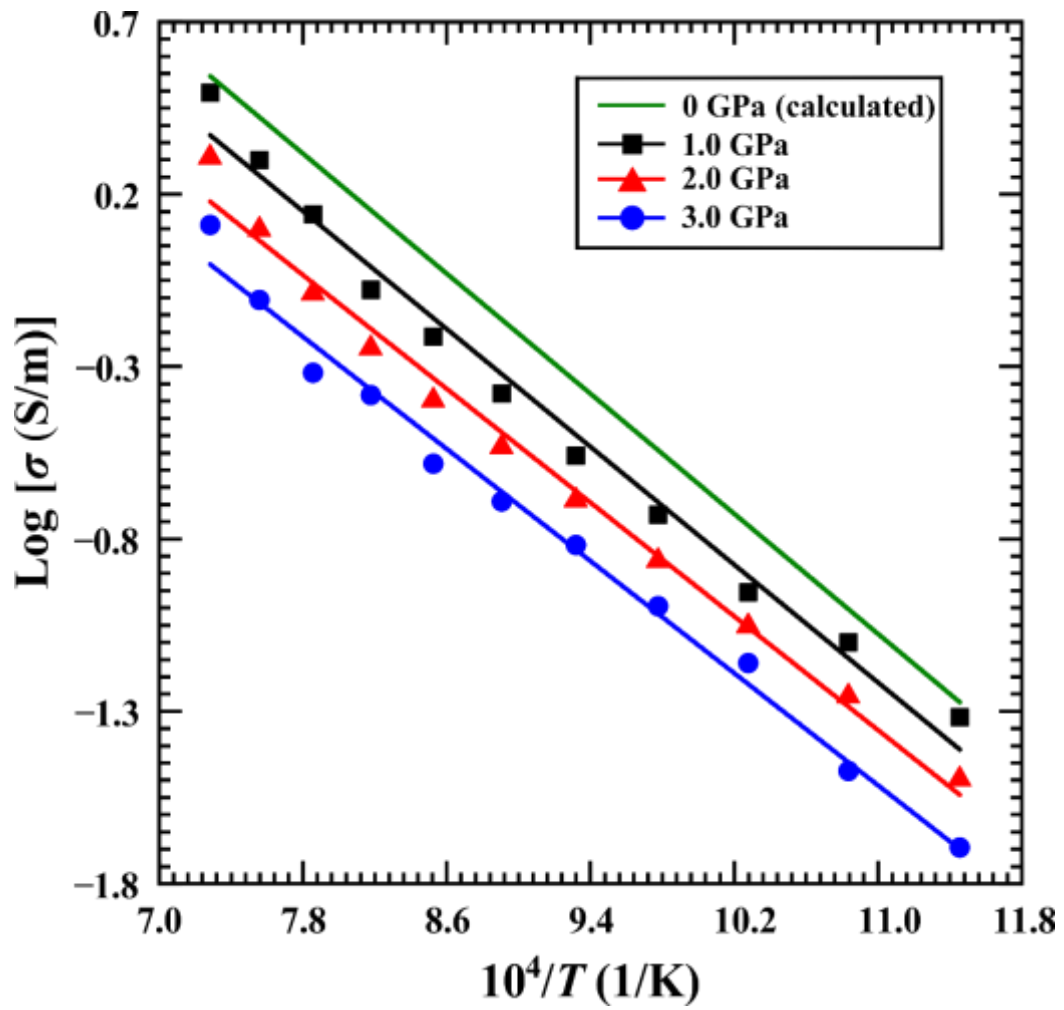
623

624 **Figure 3.** Typical complex impedance spectra for gabbroic melt with a fixed water
 625 content of 2.59 wt% at temperatures of 873–1373 K and pressure of 2.0 GPa in the
 626 frequency range from 10^0 Hz to 10^6 Hz. The fitting results for the experimental data are
 627 displayed by using the solid line.



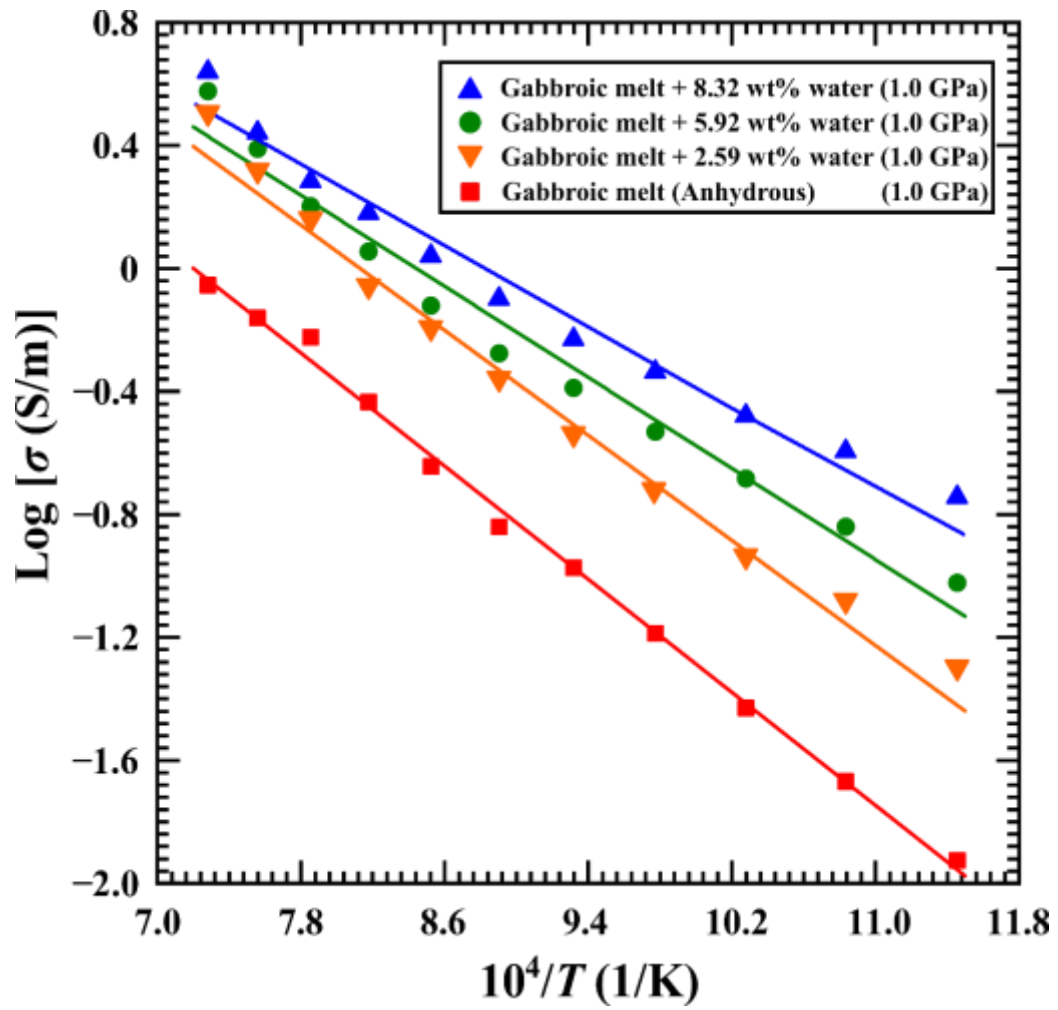
628

629 **Figure 4.** The electrical conductivity of gabbroic melt with a fixed water content of
 630 2.59 wt% among two heating–cooling cycles at a pressure of 3.0 GPa.



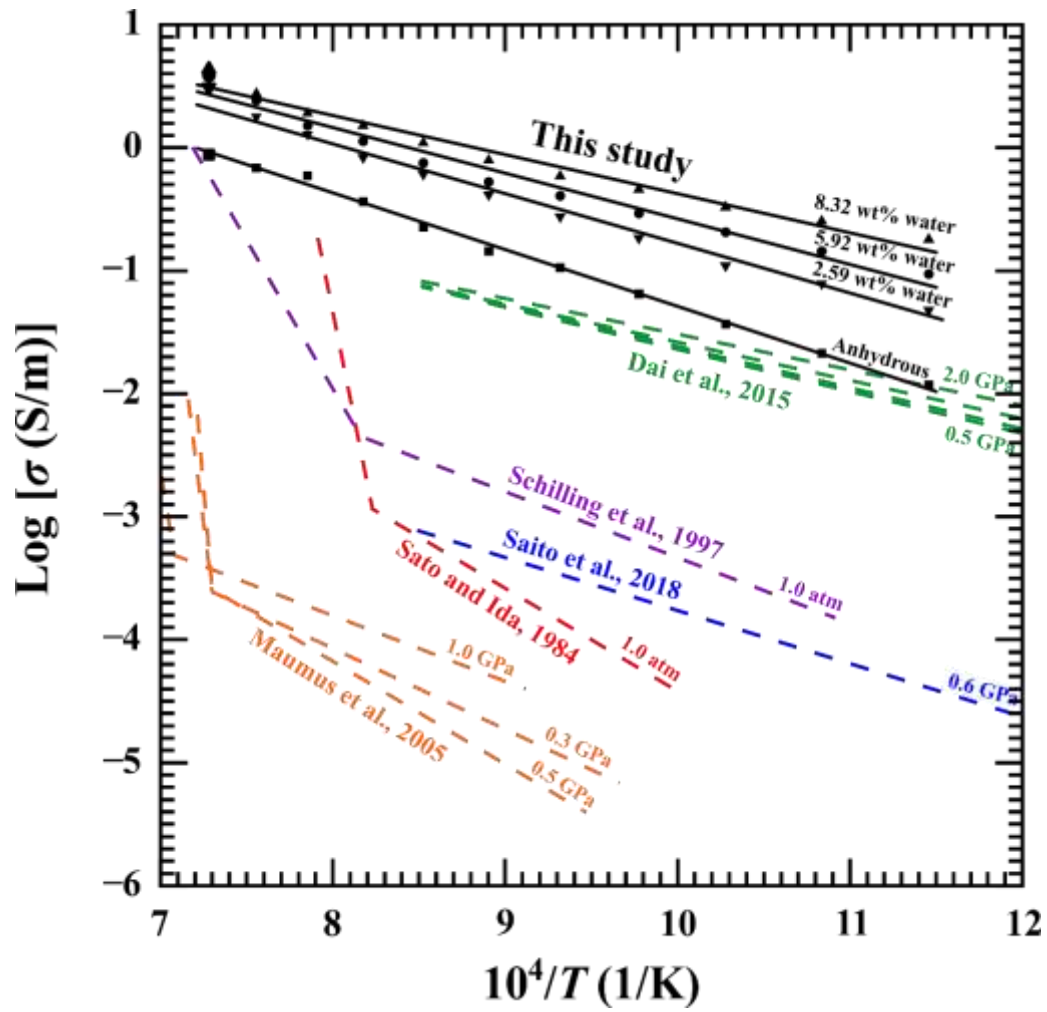
631

632 **Figure 5.** Influence of pressure on the electrical conductivity of gabbroic melt with a
 633 fixed water content of 2.59 wt% at the temperature ranges of 873–1373 K.



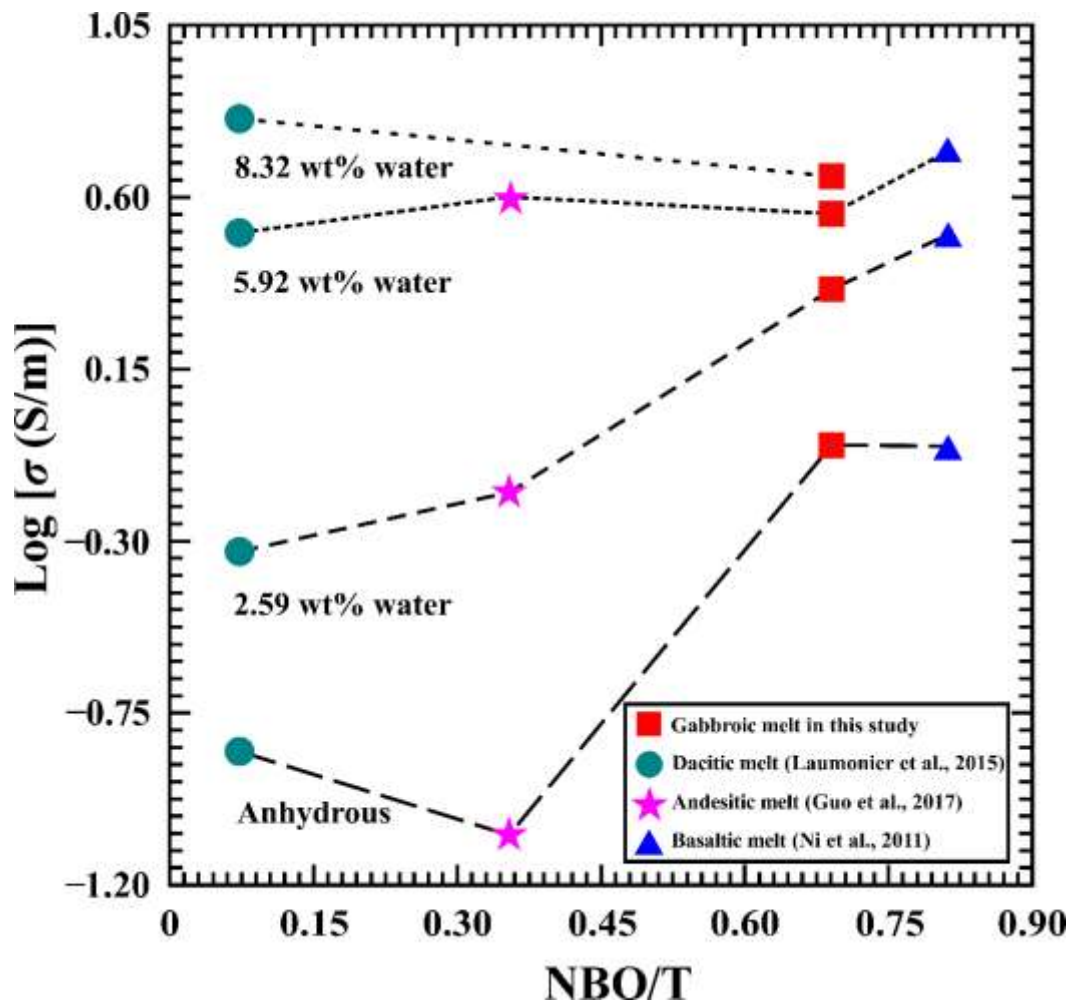
634

635 **Figure 6.** Logarithmic electrical conductivity of gabbroic melts with four different
 636 water contents as a function of reciprocal temperature at conditions of 873–1373 K and
 637 1.0 GPa.



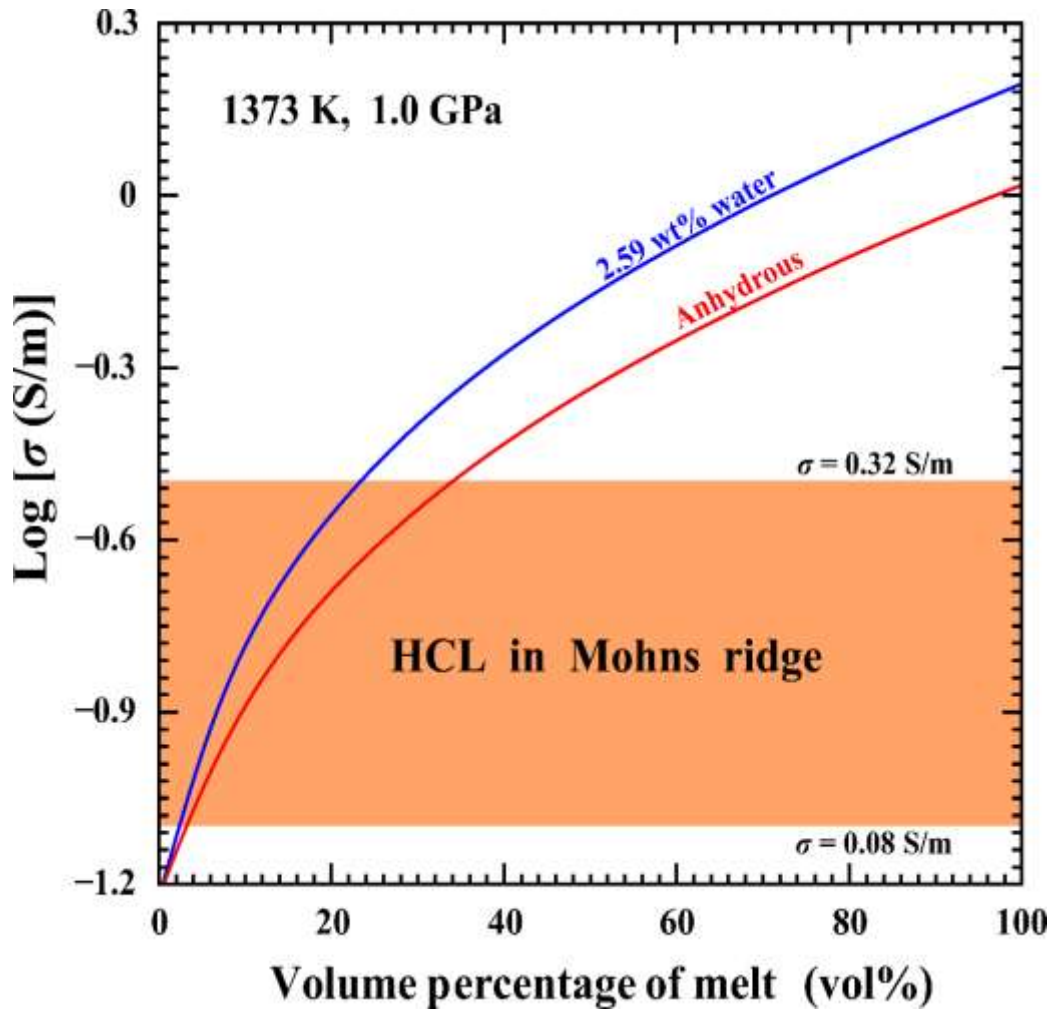
638

639 **Figure 7.** Comparison of electrical conductivity of gabbroic melts with the previously
 640 reported results from five natural gabbro samples at high-temperature and high-
 641 pressure conditions.



642

643 **Figure 8.** Variation of electrical conductivity of gabbroic melt and three representative
 644 calc-alkaline igneous rock melts with the degree of depolymerization (NBO/T) under
 645 conditions of four different water contents (i.e. 0, 2.59 wt%, 5.92 wt% and 8.32 wt%),
 646 1373 K and 1.0 GPa. Data source: basaltic melt from Ni et al. (2011), andesitic melt
 647 from Guo et al. (2017), and dacitic melt from Laumonier et al. (2015).



648

649 **Figure 9.** The electrical conductivity for the gabbroic melt–olivine system at
 650 temperature of 1373 K and 1.0 GPa, calculated with Eq. 7 of the Hashin–
 651 Shtrikman upper bound model. The electrical conductivity of olivine from Dai and
 652 Karato (2014) was adopted as σ_{olivine} . The orange region indicates the gabbro layer
 653 within the electrical conductivity range of $0.08\text{--}0.32 \text{ S m}^{-1}$ along the ultraslow–
 654 spreading Arctic mid–ocean Mohns ridge region (Johansen et al., 2019).

655 **Table 1.** The chemical composition of the gabbroic melts by virtue of the electronic
 656 probe microscopy analysis (EPMA).

Sample	SiO ₂	TiO ₂	Al ₂ O ₃	FeO	MnO	MgO	CaO	Na ₂ O	K ₂ O	Total (wt%)
Gabbroic melt (anhydrous)	51.32	0.56	12.37	9.93	0.20	11.06	11.82	2.15	0.50	99.91
Gabbroic melt (2.59 wt% water)	51.22	0.55	12.40	9.92	0.18	11.29	11.72	2.19	0.48	99.95
Gabbroic melt (5.92 wt% water)	51.23	0.57	12.40	9.87	0.18	11.28	11.70	2.21	0.47	99.91
Gabbroic melt (8.32 wt% water)	51.22	0.57	12.40	9.88	0.17	11.27	11.69	2.21	0.46	99.86

657

658 **Table 2.** Fitted parameters of Arrhenius relation for the electrical conductivity of
 659 hydrous and anhydrous gabbroic melts under conditions of 873–1373 K and 1.0–3.0
 660 GPa.

Sample	T (K)	P (GPa)	Water content Before experiment (wt%)	Water content After experiment (wt%)	Log σ_0 (σ_0 in S m ⁻¹)	ΔH (eV)
DW201	873–1373	1.0	8.32 ± 0.02	8.30 ± 0.01	2.80 ± 0.16	0.63 ± 0.03
DW204	873–1373	1.0	5.92 ± 0.01	5.90 ± 0.02	3.13 ± 0.18	0.74 ± 0.04
DW208	873–1373	1.0	2.59 ± 0.01	2.57 ± 0.01	3.48 ± 0.15	0.85 ± 0.03
DW209	873–1373	2.0	2.59 ± 0.03	2.58 ± 0.01	3.18 ± 0.13	0.83 ± 0.03
DW212	873–1373	3.0	2.59 ± 0.01	2.50 ± 0.02	2.79 ± 0.11	0.81 ± 0.03
DW210	873–1373	1.0	0	0	3.31 ± 0.08	0.93 ± 0.02

661

662 **Table 3.** Parameter values for the electrical conductivity of gabbroic melt with water
663 content of 2.59 wt% at pressures of 1.0–3.0 GPa. The equation $\sigma = \sigma_0 \cdot \exp(-\frac{\Delta U + P\Delta V}{kT})$
664 is adopted for the globally fitting of electrical conductivity data. In consideration of a
665 strong dependence of the pre-exponential factor (σ_0) on the pressure, we used the
666 relation $\sigma_0 = A_0 \cdot (1 - BP)$.

σ_0 (S m ⁻¹)	B (GPa ⁻¹)	ΔU (eV)	ΔV (cm ³ mole ⁻¹)
$A_0 = 2623.27 \pm 1.41$	$B = 0.22 \pm 0.03$	0.87 ± 0.04	-1.98 ± 0.52

667

668 **Table 4.** Parameter values for the electrical conductivity of gabbroic melts with
 669 different water contents under conditions of 873–1373 K and 1.0 GPa. The
 670 equation $\sigma = (A_1 + A_2 \cdot C_w^r) \cdot \exp\left(\frac{-\Delta H_0 - \alpha C_w^\beta}{RT}\right)$ is adopted for the globally fitting of electrical
 671 conductivity data.

A_1 (S m ⁻¹)	A_2 (S m ⁻¹)	ΔH_0 (eV)	α	β	r
6760±234	66069±240	1.03±0.04	34.85±2.24	17.70±1.31	0.43±0.05

672